Appl. Phys. B 51, 329–335 (1990)

Applied Physics B Photophysics and Laser Chemistry

Radiative and Non-Radiative Decays from the Excited State of Ti^{3+} Ions in Oxide Crystals

M. Yamaga*[,1], Y. Gao[1], F. Rasheed[1], K. P. O'Donnell[1], B. Henderson[1], and B. Cockayne[2]

[1] Department of Physics and Applied Physics, University of Strathclyde, Glasgow G4 0NG, Scotland, U.K.
[2] Royal Signal and Radar Establishment, Malvern, Worcs, WR 14 3 PS England, U.K.

Received 9 April 1990/Accepted 22 June 1990

Abstract. The fluorescence spectra of Ti^{3+} in $Y_3Al_5O_{12}$ (YAG), Al_2O_3 (sapphire), $YAlO_3$ (YAP) observed at 10 K are composed of zero-phonon lines accompanied by the broad vibronic sidebands. The temperature dependence of the fluorescence lifetime and of the total intensity of the broadband measured in YAG and Al_2O_3 indicate that the radiative decay times from the excited states are nearly constant in the range 10–300 K. This demonstrates that the broadband radiative emissions in Ti^{3+}:YAG and Ti^{3+}:Al_2O_3 are due to magnetic dipole transitions or to electric dipole transitions induced by static odd-parity distortion, respectively. The decrease of the fluorescence lifetime with increasing temperature in Ti^{3+}:YAG and Ti^{3+}:Al_2O_3 is due to non-radiative decay from the excited state which occurs through phonon-assisted tunnelling between the excited and ground states. The radiative decay of Ti^{3+}:YAP is enhanced with increasing temperature, indicating that radiative decay rate contains a term associated with odd-parity phonons. Nevertheless, a non-radiative decay rate of $3.6 \times 10^4\ s^{-1}$ observed in the temperature range 10–300 K is due to excited state absorption, which depopulates the excited state and quenches the fluorescence at the laser wavelength.

PACS: 42.70, 79.60

Laser action in Ti-sapphire (i.e. Ti^{3+}:Al_2O_3) was first reported by Moulton [1, 2]. Efficient cw laser operation of Ti^{3+} in other potential laser host crystals (e.g. $Y_3Al_5O_{12}$ (YAG) [3], $YAlO_3$ (YAP) [4, 5]) at room temperature has not been reported. That the intensity of the broadband emission of Ti^{3+} in YAG at room temperature is an order of magnitude weaker than that at 10 K [6] indicates that non-radiative decay reduces the quantum efficiency at 300 K, perhaps sufficiently to quench cw laser action at this temperature: Pulsed laser operation only has been reported [7]. In Ti^{3+}: YAP, two main absorption bands occur at the peak wavelengths of $\lambda = 432$ nm and $\lambda = 491$ nm. There is also an unexpected absorption overlapping the broadband emission with peak wavelength of 610 nm, which may be due to Ti^{3+}/Ti^{4+} pairs as was the case for sapphire [5]. The excited state absorption (ESA) coefficient was fairly weak over the wavelengths of the emission, but increased very rapidly below 520 nm [5]. This latter effect was attributed to charge transfer transition of Ti^{3+}/Ti^{4+} drastically reducing the pumping efficiency at $\lambda = 488$ nm.

We have measured the phonon structure of the emission spectra and the temperature dependence of the fluorescence lifetimes and of the total intensities of the broadband Ti^{3+} emission in YAG, sapphire, and YAP crystals. In order to examine the role played by phonon coupling in the excited and ground states as rate determining factors in radiative and non-radiative decay transitions of Ti^{3+} ions, we discuss the decay from the excited state of Ti^{3+} ions in these crystals in terms of a two-dimensional configurational coordinate model.

1. Experimental Procedure and Results

The YAG, sapphire, and YAP crystals used in this study were grown from high purity oxides using the Czochralski technique. Fluorescence emitted by Ti^{3+} ions in these crystals was excited using the 488 nm line from an Ar^+ laser and detected using a GaAs photomultiplier tube at

* Permanent address: Department of Physics, Faculty of General Education, Gifu University, Gifu 501-11, Japan

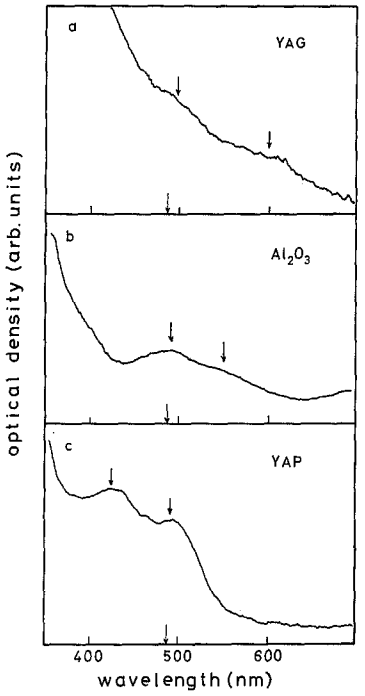

Fig. 1. Absorption spectra of Ti^{3+} in **a** YAG, **b** Al_2O_3, and **c** YAP at room temperature

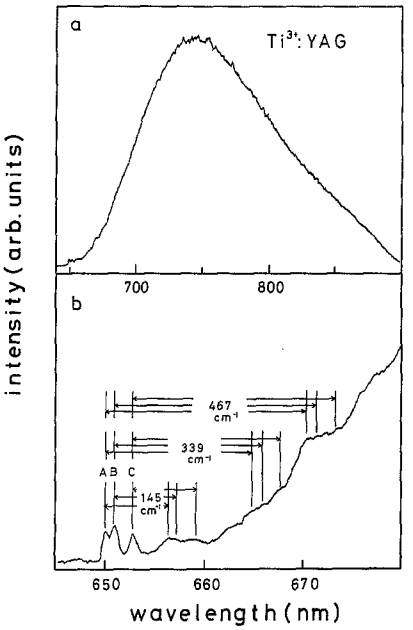

Fig. 2. **a** The emission spectrum of Ti^{3+} in YAG at 10 K. **b** Three zero-phonon lines (A, B, C) and their one-phonon sidebands at 10 K

the exit slit of a 1 m grating monochromator. The decay time of the fluorescence was measured using a boxcar averager. The samples were controlled to ± 0.1 K in the temperature range 8–300 K.

1.1. Absorption and emission spectra of Ti^{3+}

Figure 1 shows the absorption spectra of Ti^{3+} in YAG, sapphire, and YAP crystals at room temperature. The arrows indicate two overlapping peaks, whose separation yields the Jahn-Teller splitting in the excited state. Their energies are summarized in Table 1. The position of the 488 nm Ar^+ laser line is also denoted by an arrow.

Figure 2a shows the broadband emission with the peak wavelength of 750 nm of Ti^{3+} ions in YAG at 10 K. The observation of three zero-phonon lines with almost equal intensities indicates that the associated transition is

Table 1. Experimental spectral values and estimation of $10Dq$, $E_{JT}(e)$, and $\Delta E_{\pm}$ for YAG, Al_2O_3, and YAP (energy unit cm^{-1})

	YAG		Al_2O_3			YAP	
Observed							
E^-_{abs}	16700		18200			20400	
E^+_{abs}	20000		20400			23500	
E^-_{em}	13300		13500			16400	
E_{zpl}	A: 15380		A: 16230			–	
	B: 15360		B: 16190			–	
	C: 15310		C: 16120			C: 18530	
$\hbar\omega_g$	145		220			150	
	339		260			180	
	467		362			500	
						646	
ΔE	1250		2750			–	
Calculated							
$10Dq$	18350		19300			21950	
$E_{JT}(e)$	2970		3070			3420	
S_e	19.0	8.0	12.8	10.9	7.5	19.5	16.1
S_g	0.65	0.13	0.04	0.02	0.003	0.45	0.33
$\hbar\omega$	145	339	220	260	362	150	180
$S_e\hbar\omega$	2760	2710	2820	2830	2720	2930	2900
ΔE_-	26300	24200	19400	19000	18600	34200	33800
ΔE_+	9000	10800	14200	14500	16800	14400	15500

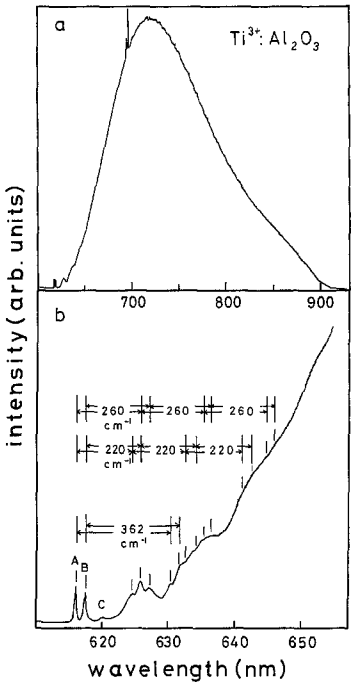

Fig. 3. a The emission spectrum of Ti^{3+} in Al_2O_3 at 10 K. **b** Three zero-phonon lines (A, B, C) and their phonon sidebands at 10 K

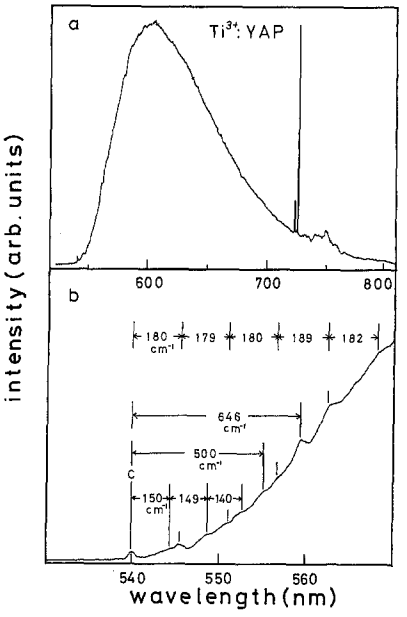

Fig. 4. a The emission spectrum of Ti^{3+} in YAP at 10 K. The spectrum in the range 725–760 nm is due to Cr^{3+} impurity ions. **b** Zero-phonon line (C) and its phonon sidebands at 10 K

magnetic dipole in origin [8, 9]. From their phonon replica, Fig. 2b, the phonon energies coupled to the ground state of the Ti^{3+} ions are estimated to be 145 cm^{-1}, 339 cm^{-1}, and 467 cm^{-1}. Figure 3a shows the broadband emission with the peak wavelength of 740 nm of Ti^{3+} ions in Al_2O_3 at 10 K. The phonon energies are estimated from the emission spectrum in Fig. 3b to be 220 cm^{-1}, 260 cm^{-1}, and 362 cm^{-1}. Figure 4a shows the broadband emission with peak wavelength of 610 nm of

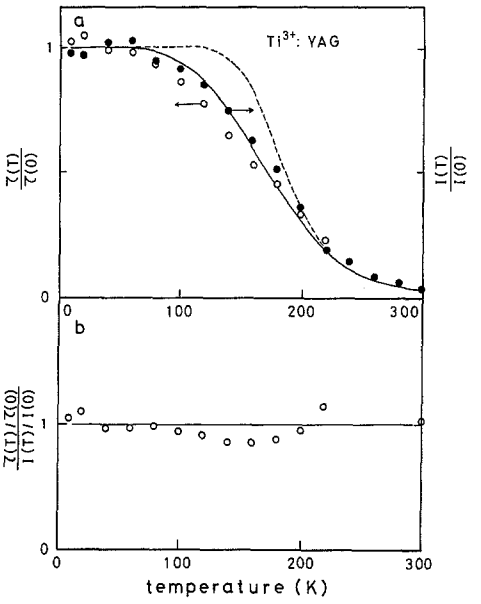

Fig. 5. a Fluorescence lifetime normalized by the lifetime $\tau(0)$ and the total intensity of the broadband normalized by $I(0)$ with the assumption that $\tau(0)$ and $I(0)$ are equal to $\tau(10)$ ($=53$ μs) and $I(10)$, respectively. The dashed curve is calculated using 15, 18, and 19 with $\tau_{st}=53$ μs, $\tau_d=\tau^0_{NR}=\infty$, $\tau^1_{NR}=5$ ns, and $\Delta E=1270\,cm^{-1}$. The solid curve is calculated using 15, 18, 20, and 21 with $\tau_{st}=53$ μs, $\tau_d=\infty$, $S_e=10$, $\hbar\omega=350\,cm^{-1}$, $R_{NR}=4\times10^{14}\,s^{-1}$, and $p=36.5$. **b** The ratio of the normalized lifetime to the normalized intensity, $[\tau(T)/\tau(0)]/[I(T)/I(0)]$. The solid line represents a ratio equal to one

Ti^{3+} ions in YAP at 10 K. The emission lines in the range 725–755 nm are due to the R-lines and their phonon sideband from Cr^{3+} impurity ions. The single zero-phonon line ($\lambda=539.7$ nm) and its phonon replica at the short wavelength tail of the broadband are shown in Fig. 4b. The analysis of the polarization of zero-phonon line emission was reported in [8, 9]. The energies of phonons are estimated to be 150 cm^{-1}, 180 cm^{-1}, 500 cm^{-1}, and 646 cm^{-1}.

1.2. Lifetime and intensity of broadband emission of Ti^{3+}

Figure 5a shows the normalized total intensity, $I(T)/I(0)$, and normalized fluorescence lifetime, $\tau(T)/\tau(0)$, of the broadband in Ti^{3+}:YAG as a function of temperature. The lifetime, $\tau(T)$ at $T=10$ K is 53 μs and that at 300 K is about 2 μs [3]. Both quantities show the same temperature dependence. The ratio of the normalized lifetime to the normalized intensity is almost unity in the range 10–300 K, Fig. 5b, as is expected for radiative decay from the Ti^{3+} excited state. Figure 6 shows the temperature dependence of the intensity and lifetime and their ratio in $Ti^{3+}:Al_2O_3$. The lifetime data were taken from [2]. The lifetime $\tau(T)$ at $T=20$ K is 3.8 μs. The intensity data above 300 K were reported in [10]. This behaviour is very similar to that for YAG except that the temperature at

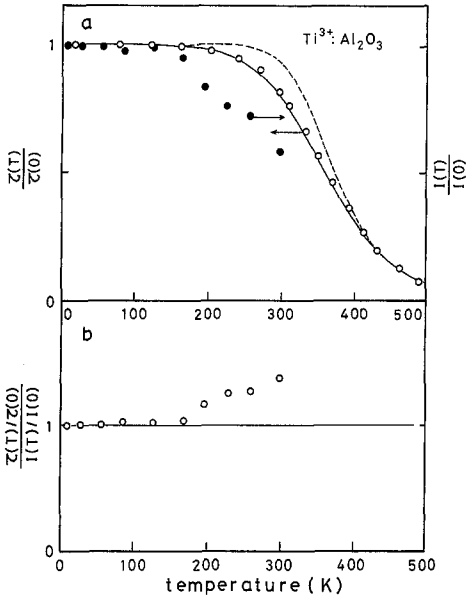

Fig. 6. a Fluorescence lifetime normalized by the lifetime $\tau(0)$ and the total intensity of the broadband normalized by $I(0)$ with the assumption that $\tau(0)$ and $I(0)$ are equal to $\tau(20)$ ($=3.8\,\mu s$) and $I(10)$, respectively. The lifetime data $\tau(T)$ are reproduced from [2]. The dashed curve is calculated using $\tau_{st}=3.8\,\mu s$, $\tau_d=\tau^0_{NR}=\infty$, $\tau^1_{NR}=100\,ps$, and $\Delta E=2750\,cm^{-1}$. The solid curve is calculated using $\tau_{st}=4\,\mu s$, $S_e=10$, $\hbar\omega=350\,cm^{-1}$, $R_{NR}=4\times10^{14}\,s^{-1}$, and $p=39$. **b** The ratio of the normalized lifetime to the normalized total intensity, $[\tau(T)/\tau(0)]/[I(T)/I(0)]$. The solid line represents a ratio equal to one

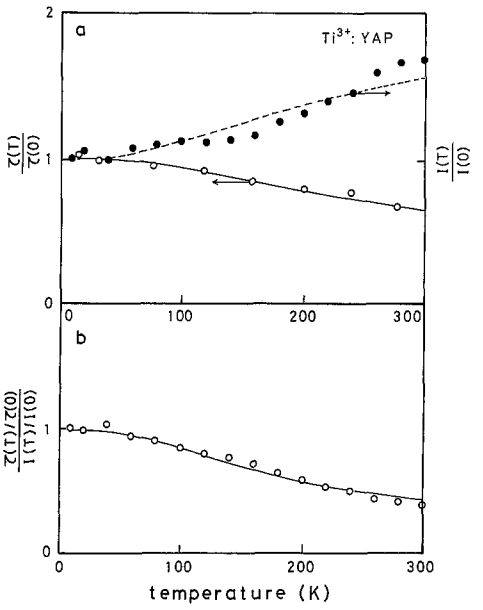

Fig. 7. a Fluorescence lifetime normalized by the lifetime $\tau(0)$ and the total intensity of the broadband normalized by $I(0)$ with the assumption that $\tau(0)$ and $I(0)$ are equal to $\tau(15)$ ($=17\,\mu s$) and $I(10)$, respectively. The lifetime data $\tau(T)$ are reproduced from [4]. The solid and dashed curves are fitted to the lifetime, $\tau(T)/\tau(0)$, and the intensity, $I(T)/I(0)$, using (15, 16, 18, and 19) with $\tau_{st}=187\,\mu s$, $\tau_d=56\,\mu s$, $\tau^0_{NR}=28\,\mu s$, $\tau^1_{NR}=\infty$, and $\hbar\omega=150\,cm^{-1}$, respectively. **b** The ratio of the normalized lifetime to the normalized intensity, $[\tau(T)/\tau(0)]/[I(T)/I(0)]$. The solid curve is calculated using (18) with $\tau_{st}:\tau_d=10:3$ and $\hbar\omega=150\,cm^{-1}$

which the intensity and lifetime start to decrease is a little higher than that in YAG. Figure 7a shows the temperature dependence of the normalized total intensity and fluorescence lifetime of the broadband in Ti^{3+}: YAP. The lifetime data are reproduced from [4]. The lifetime, $\tau(T)$, at $T=15$ K is 17 μs. The total intensity at 300 K is about 1.7 times larger than that at 10 K. Figure 7b shows the ratio of the normalized lifetime to the normalized intensity as a function of temperature. The ratio decreases above 100 K.

2. Discussion

2.1. Two-Dimensional Configuration Coordinates

The Ti^{3+} ion has the $3d^1$ electron configuration. In octahedral arrays of ligand ions the free-ion ^2D state splits into three-fold, $^2T_{2g}$, and two-fold, ^2E_g, orbitally degenerate states with energy separation, $10Dq$, both of which undergo Jahn-Teller distortion. Although both, E_g and T_{2g}, distortion modes couple to these states, the E_g-mode is dominant. The Jahn-Teller coupling coefficient of the E_g-mode for the ^2E_g state is much larger than that for the $^2T_{2g}$ state, because e_g orbitals are extended towards ligand ions. The Jahn-Teller distortion energy is $E_{JT}=V^2/2M\omega^2$, where V is the Jahn-Teller coupling coefficient, M the ligand mass and ω the vibration frequency of the E_g mode. The distortion energy is given by $S\hbar\omega$, where S is the Huang-Rhys factor. The values of E_{JT} for the ground and excited states of Ti^{3+} in Al_2O_3 were estimated to be 200 cm^{-1} [11] and 3000 cm^{-1} [12], respectively. Here, we consider spectral values (peak energies of broadband of absorption and emission, zero-phonon lines and activation energies) of Ti^{3+} in oxide crystals in terms of two-dimensional configuration coordinates of the Jahn-Teller E_g-mode.

First, we consider the Jahn-Teller coupling of phonons of E_g symmetry, which may be measured directly from Raman and infrared (IR) spectra: the A_{1g}, E_g, T_{2g}-modes are Raman-active, whereas T_{1u}-modes are IR-active. Phonon energies obtained from the emission spectrum of Ti^{3+}:YAG (145 cm^{-1} and 339 cm^{-1}) are close to those (162 cm^{-1} and 340 cm^{-1}) of E_g-mode phonon measured from the Raman spectrum [13]. In $Ti^{3+}:Al_2O_3$ also the phonon energies determined from the luminescence spectrum in Fig. 3b (i.e. 220 cm^{-1} and 260 cm^{-1}) are similar to those (190 cm^{-1} and 265 cm^{-1}) determined from the Raman spectrum [14]. The phonon energies of the Jahn-Teller E_g-mode in oxide crystals are in the range 100–500 cm^{-1}.

Figure 8 shows a schematic configurational coordinate diagram for Ti^{3+}. The orbitally degenerate excited and ground states are split into upper (E_+) and lower (E_-) branches, respectively, by the Jahn-Teller effect with energies given by

ground state $^2T_{2g}$:

$$E^g_{\pm}(R)=S_g\hbar\omega_g(1\pm R/R^g_0)^2-S_g\hbar\omega_g, \quad (1)$$

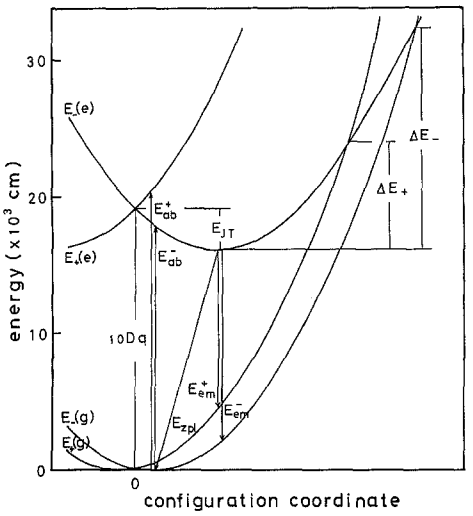

Fig. 8. Schematic diagram of configuration coordinates of Ti^{3+}. The observed values of $E^{\pm}_{abs}$, E^{-}_{em}, and E_{zpl} and the estimated values of $10Dq$, E_{JT}, and $\Delta E_{\pm}$ for YAG, Al_2O_3, and YAP are summarized in Table 1

excited state ^2E_g:

$$E^{e}_{\pm}(R)=10Dq+S_e\hbar\omega_e(1\pm R/R^{e}_0)^2-S_e\hbar\omega_e, \tag{2}$$

where

$$R^{i}_0=\sqrt{\frac{2S_i\hbar}{M\omega_i}}\,(i=g,e), \tag{3}$$

S_i and $\hbar\omega_i$ $(i=g,e)$ are the Huang-Rhys factor and the phonon energy of the E_g-mode for the ground and excited states and R is a distortion coordinate.

The radial part of the two-dimensional vibrational ground state wavefunction, $\Phi_i(R,\theta)=\phi_i(R)\psi_i(\theta)$ $(i=g,e)$, coupled to the lower branches of the ground and excited electronic states is represented by

$$\phi_i(R)=\left(\frac{\alpha_i}{\sqrt{\pi}}\right)^{1/2}\exp\left[-\frac{\alpha_i^2}{2}(R-R^{i}_0)^2\right], \tag{4}$$

$$\alpha_i=\sqrt{\frac{M\omega_i}{\hbar}}\quad(i=g,e). \tag{5}$$

The probability distribution of the coordinate R [15] is maximal at

$$R^{i}_m=\frac{1}{\sqrt{2\alpha_i}}\quad(i=g,e). \tag{6}$$

The optical absorption and emission transitions in the Frank-Condon approximation occur at energies given by the separation between $E^{e}_{\pm}(R)$ at $R=R^{g}_0+R^{g}_m$ and $E^{g}_{-}(R)=-(S_g-1)\hbar\omega$ and between $E^{g}_{\pm}(R)$ at $R=R^{e}_0+R^{e}_m$ and $E^{e}_{-}(R)=10Dq-(S_e-1)\hbar\omega$ may, with the assumption that $\omega=\omega_g=\omega_e$, be written as

$$E^{\pm}_{abs}=10Dq+(2S_g+\sqrt{S_g}\pm\sqrt{S_e}\pm2\sqrt{S_gS_e}-3/4)\hbar\omega, \tag{7}$$

$$E^{\pm}_{em}=10Dq-(2S_e+\sqrt{S_e}\pm\sqrt{S_g}\pm2\sqrt{S_gS_e}-3/4)\hbar\omega. \tag{8}$$

The zero-phonon transition energy, E_{zpl}, is given by

$$E_{zpl}=10Dq+(S_g-S_e)\hbar\omega. \tag{9}$$

We rewrite $10Dq$ and (S_g,S_e) using (7) and (8) as

$$10Dq=\tfrac{1}{2}(E^{+}_{abs}+E^{-}_{abs})-(2S_g+\sqrt{S_g}-3/4)\hbar\omega \tag{10}$$

$$\sqrt{S_e}=\frac{E^{+}_{abs}-E^{-}_{abs}}{2(1+2\sqrt{S_g})\hbar\omega}, \tag{11}$$

$$\sqrt{S_e}-\sqrt{S_g}=\sqrt{\frac{E^{-}_{abs}-E^{-}_{em}}{2\hbar\omega}+\frac{3}{4}}. \tag{12}$$

The value of $10Dq$ is in the range 18 000–22 000 cm^{-1} and the value of $E_{JT}(g)=S_g\hbar\omega$ is typically 100–300 cm^{-1}. Therefore, $10Dq$ may be approximated by the first term of(10), that is, the average of the peak energies of two separated absorption bands. The Jahn-Teller energy of the excited state, $E_{JT}(e)$, can also be estimated approximately from the observed absorption and zero-phonon emission lines with an assumption that $S_g=0$ and is

$$E_{JT}(e)=S_e\hbar\omega=\tfrac{1}{2}(E^{+}_{abs}+E^{-}_{abs})-E_{zpl}. \tag{13}$$

Activation energies $\Delta E_{\pm}$ for non-radiative decays in Fig. 8 are given by

$$\Delta E_{\pm}=\hbar\omega\left(\frac{10Dq}{2\hbar\omega}\frac{1}{\sqrt{S_e}\pm\sqrt{S_g}}-\sqrt{S_e}\right)^2. \tag{14}$$

Next, we estimate the values if $10Dq$, S_g, S_c, $\hbar\omega$, and $\Delta E_{\pm}$. The observed values of $E^{\pm}_{abs}$, E^{-}_{em}, E_{zpl}, and $\hbar\omega_g$ in Ti^{3+}:YAG, sapphire, and YAP are summarized in Table 1. The value of $10Dq$ is the average of E^{+}_{abs} and E^{-}_{abs}. The Jahn-Teller energies, $E_{JT}(e)$, in Table 1 are obtained using (13). The values of S_e and S_g are calculated using (11) and (12) with the observed values of $E^{\pm}_{abs}$, E^{-}_{em}, and $\hbar\omega_g$. The difference between $E_{JT}(e)$ and $S_e\hbar\omega$ calculated separately may be due to the band peak energies of absorption and emission being accurate only to within $\pm5\%$. The values of $\Delta E_{\pm}$ are estimated using (14) and the values of $10Dq$, S_g, S_e, and $\hbar\omega$; they are included in Table 1.

2.2. *Radiative and Non-Radiative Decays*

The observed fluorescence lifetime and the total intensity of the broadband at temperature, T, are written as

$$\frac{1}{\tau(T)}=\frac{1}{\tau_R(T)}+\frac{1}{\tau_{NR}(T)}, \tag{15}$$

$$I(T)=I_0\frac{\tau(T)}{\tau_R(T)}, \tag{16}$$

where $\tau_R(T)$ and $\tau_{NR}(T)$ are radiative and non-radiative decay times. From (15) and (16), the ratio, $R(T)$, of the normalized decay time, $\tau(T)/\tau(0)$, to the normalized intensity, $I(T)/I(0)$, is written as

$$R(T)\equiv\frac{\tau(T)/\tau(0)}{I(T)/I(0)}=\frac{\tau_R(T)}{\tau_R(0)}, \tag{17}$$

which represents implicitly the radiative decay time.

The radiative and non-radiative decay rates contain temperature-independent and temperature-dependent terms:

$$\frac{1}{\tau_R(T)} = \frac{1}{\tau_{st}} + \frac{1}{\tau_d}\coth(\hbar\omega/2kT), \tag{18}$$

$$\frac{1}{\tau_{NR}(T)} = \frac{1}{\tau_{NR}^0} + \frac{1}{\tau_{NR}^1}\exp(-\Delta E/kT). \tag{19}$$

The first term, $1/\tau_{st}$, on (18) represents contributions to the decay rate from magnetic dipole transitions or from electric dipole transitions which have been induced by static odd-parity crystal distortion. The second term is a dynamic term induced by odd-parity phonons with the frequency ω. The first non-radiative term, $1/\tau_{NR}^0$, in (19) is due to non-radiative energy transfer to other electronic energy levels at the same or other sites and which is independent of temperature. The second term in (19) is associated with non-radiative transitions to the ground state for which the thermal activation energy ΔE is shown in Fig. 8. As the activation energy is reduced, tunnelling occurs between the ground and excited states [16–18]. The second term in (19) is then replaced by

$$R_{NR}\sum_{m=0}^{\infty}(1-r)r^m|\langle\phi_e(R)|\phi_g(R)\rangle|^2$$
$$= R_{NR}\exp(-S_e\langle 2m+1\rangle)(2\pi y_p)^{-\frac{1}{2}}$$
$$\times\exp(y_p)[2S_e\langle 1+m\rangle/(p+y_p)]^p, \tag{20}$$
$$y_p = (p^2+4S_e^2\langle 1+m\rangle\langle m\rangle)^{\frac{1}{2}},$$
$$\langle m\rangle = r/(1-r), \tag{21}$$
$$r = \exp(-\hbar\omega/kT),$$

where $\langle m\rangle$ is the average thermal occupancy of the vibrational states and p denotes the number of phonons created. This analysis is now applied to the radiative and non-radiative decays from the excited states of Ti^{3+} in YAG, Al_2O_3, and YAP.

(i) Ti^{3+}:YAG

The octahedral site in YAG occupied by Ti^{3+} ions is distorted along the crystal $\langle 111\rangle$ axis. However, the distortions are of even-parity so that the site retains inversion symmetry. The transition from the excited state ^2E_g to the ground state $^2T_{2g}$ is spin-allowed, but parity-forbidden. The observed fluorescence lifetime (53 μs) of Ti^{3+} in YAG at 10 K is an order of magnitude longer than in Al_2O_3 (3.8 μs), and as shown in Fig. 5a is constant with temperature in the range 10–100 K, but decreases above 100 K. However, the value of $R(T)$ in (17) is almost constant up to 300 K (Fig. 5b) within ±10% experimental error. The contribution to the change of $R(T)$ from the temperature dependence of the absorption coefficient at the pumping wavelength 488 nm, which is located in the shorter wavelength tail of upper branch absorption in Fig. 1, is negligible. In addition, the relative intensities of the three zero-phonon lines are equal to each other. These experimental results show that for Ti^{3+}:YAG the radiative decay ($1/\tau_{st}$) is due to magnetic dipole processes and that effects due to odd-parity phonons are negligible. The decrease in the lifetime above 100 K is due to non-radiative decay. The dashed curve in Fig. 5a is calculated using (15, 18, 19) with $\tau_{st}=53$ μs, $\tau_d=\tau_{NR}^0=\infty$, $\tau_{NR}^1=5$ ns, and $\Delta E=1270\ cm^{-1}$. The high quantum efficiency of the fluorescence requires that $E_{JT}<\Delta E$ [19]. The estimated value of ΔE ($1250\ cm^{-1}$) does not satisfy this relation, whereas the $\Delta E_{\pm}$ in Table 1 calculated using (14) are reasonable. The discrepancy between the observed and calculated values can be explained in terms of tunnelling between the excited and ground states. The solid curve in Fig. 5a calculated using (15, 18, 20, 21) with $\tau_{st}=53$ μs, $\tau_d=\infty$, $S_e=10$, $\hbar\omega=350\ cm^{-1}$, $R_{NR}=4\times10^{14}\ s^{-1}$, and $p=36.5$ is in excellent agreement with experimental data. The fitting parameters; $S_e=10$, $\hbar\omega=350\ cm^{-1}$, and $E_{JT}(e)=3500\ cm^{-1}$, are also in agreement with those estimated from the optical data in Table 1.

(ii) Ti^{3+}:Al_2O_3

The short lifetime (3.8 μs) at 20 K is due to electric dipole transition induced by odd-parity distortion [8, 9]. The ratio $R(T)$ given by (17) and plotted in Fig. 6b increases with increasing temperature above 200 K, which is unexpected, since the radiative decay time should either be constant or decrease at high temperatures as shown in (15) and (18). This may be due to the change of the absorption coefficient at the pumping wavelength 488 nm which is located near the peak of the upper branch absorption in Fig. 1. In general, absorption spectra for localized luminescent centres are red-shifted and broadened by lattice dilation with increasing temperature. This effect may reduce the 488 nm absorption coefficient at room temperature compared to that at low temperatures; the fluorescence efficiency may thus be decreased at room temperature. Here, assuming that the radiative decay rate is constant in the range 10–400 K and equal to $1/\tau_{st}$, the temperature dependence of the lifetime is expected to be similar to that of Ti^{3+}:YAG. In Fig. 6a, the dashed curve is calculated using $\tau_{st}=3.8$ μs, $\tau_d=\tau_{NR}^0=\infty$, $\tau_{NR}^1=100$ ps, and $\Delta E=2750\ cm^{-1}$, whereas the solid curve is calculated using $\tau_{st}=4$ μs, $S_e=10$, $\hbar\omega=350\ cm^{-1}$, $R_{NR}=4\times10^{14}\ s^{-1}$, and $p=39$. Fair agreement is obtained between calculated and experimental data. The only difference in the fitting parameters determined for Ti^{3+}:YAG and Ti^{3+}:Al_2O_3 is in p, the average number of phonons created, the same phonon energy having been adopted for these materials and which is proportional to optical transition energy (E_{em}^-). When $10Dq$ decreases from Al_2O_3 to YAG, assuming $E_{JT}(e)$ to be constant, the activation energy $\Delta E_{\pm}$ becomes reduced and tunnelling between ground and excited states occurs more easily.

(iii) Ti^{3+}:YAP

The total intensity of the broadband at 300 K is enhanced by a factor of 1.7 compared to that at 10 K as shown in

Fig. 7a. Here, we assume that the absorption coefficient at the pumping wavelength 488 nm, being located between two absorption bands as shown in Fig. 1, is constant in the range of 10–300 K as in the case of Ti^{3+}:YAG. The data for $R(T)$, in Fig. 7b, show directly the radiative decay time, $\tau_R(T)$. The decrease of $\tau_R(T)$ is due to the odd-mode phonon-assisted radiative transition. The solid curve in Fig. 7b is fitted to the observed ones using (18) with $\tau_{st}:\tau_d = 10:3$ and $\hbar\omega = 150\ cm^{-1}$. The phonon frequency is that obtained from the phonon-structure in the emission spectrum. When the phonon frequency increases, the temperature at which the fluorescence lifetime decreases is higher. The other observed phonon frequency ($180\ cm^{-1}$) does not give a good fit to the observed lifetime data. The solid and dashed curves in Fig. 7a are fitted to experimental fluorescence lifetime, $\tau(T)/\tau(0)$, and total intensity, $I(T)/I(0)$, data using (15, 16, 18, 19) with $\tau_{st} = 187\ \mu s$, $\tau_d = 56\ \mu s$, $\tau_{NR}^0 = 28\ \mu s$, $\tau_{NR}^1 = \infty$, and $\hbar\omega = 150\ cm^{-1}$, respectively. Here, the temperature-independent non-radiative decay rate is larger than the radiative decay rate at low temperature. Since the radiative decay rate is enhanced by odd-parity phonons as temperature increases, the total intensity increases at room temperature. However, Wegner and Petermann [5] have shown that non-radiative decay occurs through excited state absorption involving transitions from the lowest excited ^2E_g level to higher lying charge transfer states with energy separation at the pump energy (i.e. the 488 nm Ar^+ ion line). Excited state absorption depopulates the ^2E_g level so that increasing pump power may cause strong fluorecence quenching.

3. Conclusions

The fluorescence spectra of Ti^{3+} in YAG, Al_2O_3, and YAP observed at 10 K are composed of the zero-phonon lines accompanied by the broad vibronic sidebands. The frequencies of phonons coupled to the ground state have been estimated from the fluorescence band shape. The temperature dependence of the fluorescence lifetime and the total intensities of the broadband in these materials have also been measured. The ratio of the normalized lifetime to the normalized intensity in YAG and sapphire are nearly constant in the range 10–300 K. However, the decrease of the fluorescence lifetime between 80–300 K is due to non-radiative decay. The radiative transition in the broadband for Ti^{3+}:YAG is due to magnetic dipole processes as is indicated by the long radiative lifetime $\tau_R = 53\ \mu s$ at 10 K; in $Ti^{3+}:Al_2O_3$ the fluorescence is via electric dipole transitions and the lifetime at 20 K, $\tau_R = 3.8\ \mu s$ is an order of magnitude shorter than in Ti^{3+}:YAG. Non-radiative decay from the excited state of Ti^{3+}:YAG and $Ti^{3+}:Al_2O_3$ occurs through phonon-assisted tunnelling between excited and ground states. The frequencies of phonons coupled to the electronic levels in YAG and Al_2O_3 are about $350\ cm^{-1}$, equal to those obtained from the fluorescence spectra. The difference in the temperatures at which the fluorescence lifetimes begin to decrease in YAG and Al_2O_3 can be explained in terms of optical transition energy being proportional to $10Dq$: when $10Dq$ decreases under the assumption that Jahn-Teller energy is constant, the activation energy for non-radiative decay is reduced and so too is the number of phonons excited in the decay process. Tunnelling between the ground and excited states then occurs more easily.

The radiative decay rate of Ti^{3+}:YAP is enhanced with increasing temperature, indicating that the radiative decay rate contains a term due to phonon-assisted transition induced by odd-parity phonons, being proportional to $\coth(\hbar\omega/2kT)$. The odd-parity phonon frequency estimated from the temperature dependence of the radiative decay time is $150\ cm^{-1}$, equal to that inferred from peaks in the fluorescence spectrum. In addition, a temperature-independent non-radiative decay rate of $3.6 \times 10^4\ s^{-1}$ is observed in the range 10–300 K, which may be due to the excited state absorption (ESA) at the pump wavelength of the 488 nm Ar^+ ion line. The consequent depopulation of the excited state quenches the fluorescence, and hence, the laser action.

Acknowledgements. One of the authors (M. Yamaga) is indebted to SERC for a senior visiting fellowship in 1989 and the INAMORI foundation for financial support. In general, the work at the university is supported by the SERC and the Ministry of Defence. The authors are indebted to J.G. Plant and M.J. Crosbie for assistance in growing the crystals.

References

1. P. Moulton: Optics News **8**, 9 (1982)
2. P. Moulton: J. Opt. Soc. Am. B **3**, 125 (1986)
3. F. Bantien, P. Albers, G. Huber: J. Lumin. **36**, 363 (1986)
4. K.L. Schepler: In *Tunable Solid-State Lasers* II, ed. by A.B. Budgor, L. Esterowitz, L.G. DeShazer (Springer, Berlin, Heidelberg 1986) p. 235
5. T. Wegner, K. Petermann: Appl. Phys. B **49**, 275 (1989)
6. F. Rasheed: *PhD Thesis*, University of Strathclyde (1989)
7. T.A. Driscoll, M. Peressini, R.E. Stone, G. Hansen, H.J. Hoffman: *Digest of Technical Papers, Conference on Lasers and Electro Optics* (San Francisco 1986) p. 106
8. M. Yamaga, B. Henderson, K.P. O'Donnell: Appl. Phys. B (to be published)
9. M. Yamaga, B. Henderson, F. Rasheed, K.P. O'Donnell, Y. Gao, B. Cockayne: Appl. Phys. B (to be published)
10. A. Sanchez, R.E. Fahey, A.J. Strauss, R.L. Aggrawal: In *Tunable Solid-State Lasers* II, ed. by A.B. Budgor, L. Esterowitz, L.G. DeShazer (Springer, Berlin, Heidelberg 1986) p. 202
11. R.M. Macfarlane, J.Y. Wong, M.D. Sturge: Phys. Rev. **166**, 250 (1968)
12. D.S. McClure: J. Chem. Phys. **36**, 2757 (1962)
13. J.P. Hurrell, S.P.S. Porto: Phys. Rev. **173**, 851 (1968)
14. R.C. Powell: In *Tunable Solid-State Lasers*, ed. by P. Hammerling, A.B. Budgor, A. Pinto (Springer, Berlin, Heidelberg 1985) p. 60
15. M.D. Sturge: *The Jahn-Teller Effect in Solids*, ed. by F. Seitz, D. Turnbull, H. Ehrenriech, Solid State Physics, Vol. 20 (Academic, New York 1968) p. 188
16. W.H. Fonger, C.W. Struck: J. Chem. Phys. **69**, 4171 (1978)
17. C.W. Struck, W.H. Fonger: J. Lumin. **18/19**, 105 (1970)
18. P. Albers, E. Stark, G. Huber: J. Opt. Soc. Am. B **3**, 134 (1986)
19. B. Henderson, G.F. Imbusch: *Optical Spectroscopy of Inorganic Solids* (Clarendon, Oxford 1989) p. 245